Low-Frequency Electrical Properties of Ice−Silicate Mixtures

David E. Stillman,*,† Robert E. Grimm,† and Steven F. Dec‡

Department of Space Studies, Southwest Research Institute, 1050 Walnut St. #300, Boulder, Colorado 80302, and Department of Chemistry and Geochemistry, Colorado School of Mines, 1500 Illinois Street, Golden, Colorado 80401

The low-frequency electrical properties of mixtures of silicates and saline H_2O were measured over broad ranges of temperature and frequency to assess the subfreezing interactions between these materials synoptically, particularly the effects of adsorbed, unfrozen water. Adsorbed water content was determined using nuclear magnetic resonance. Materials were chosen to control effects of grain size and mineralogical complexity, and the initial salt content was also specified. The temperature-dependent DC conductivity of a sand−salt−H_2O mixture was found to be described well by Archie's law, with either brine or salt hydrate (above and below the eutectic, respectively) as the conductive and partially saturating phase. For materials with pore sizes less than a few micrometers, the brine/hydrate channels become disconnected, and the DC conductivity is controlled by the surrounding ice. High DC conductivity in a montmorillonite−H_2O mixture is attributed to proton mobility in interlayer adsorbed water. The ice content of the sand mixture was recovered from the static dielectric permittivity using a power-law mixing model. Ice relaxation frequencies were higher than those observed in defect-saturated saline ice, indicating that additional defects are able to form in proximity to silicate surfaces. Five dielectric relaxations related to H_2O were identified: two orientation polarizations (ice and adsorbed water), two Maxwell−Wagner interfacial polarizations (because of the conductivity differences between hydrate and silicate and adsorbed water and ice, respectively), and a low-frequency dispersion, probably caused by charge hopping. Thicknesses of a few H_2O monolayers and the preference of hydronium for surface sites, making adsorbed water slightly acidic, favor protons as the mobile charges responsible for these adsorbed-water interfacial polarizations.

1. Introduction

The physical interaction between H_2O and solid surfaces is a subject of abiding interest.[1,2] In earth and planetary science, silicates are the most common substrate for H_2O, and their interaction causes capillary flow of water both above and below freezing temperatures.[3,4] Indeed, subfreezing interfacial melting, or "unfrozen" water, is responsible for a variety of periglacial landforms.[4,5] Ice and adsorbed water have unique electrical properties that may allow noninvasive geophysical techniques, such as ground-penetrating radar and geoelectrical methods,[6] to map their distribution in the subsurface. To provide a framework for geophysical measurements, we sought to measure and identify the causes of electrical signatures in ice−silicate mixtures over a frequency range of 1 mHz to 1 MHz and a temperature range of 180−298 K. Nuclear magnetic resonance (NMR) was used to determine the abundance of unfrozen water. Our results have fundamental implications for the geometry and mechanisms of charge transport in subfreezing H_2O−silicate mixtures.

2. Background

The complex dielectric permittivity $\varepsilon^* = \varepsilon' - i\varepsilon''$ ($i = \sqrt{-1}$) describes how a material stores (ε') and dissipates (ε'') electrical energy. When an external electrical field is applied, free and bound charges move in response. Free charges dissipate kinetic energy during collisions as they migrate in response to the electric field. This loss is expressed as the DC electrical conductivity, σ_{DC}, and makes a contribution, $\sigma_{DC}/\omega\varepsilon_0$, to the imaginary permittivity, where ω is the angular frequency and ε_0 is the dielectric permittivity of vacuum. Bound charges create induced dipoles and give rise to electronic, atomic, and Maxwell−Wagner interfacial polarizations. Permanent dipoles rotate to align their moment against the applied field creating orientational polarization. Induced and permanent dipoles store energy when their moments are antiparallel to the applied electric field (ε') and dissipate energy when they are out of phase with the applied electric field (ε'').

The complex permittivity becomes frequency-dependent when dipoles can no longer stay in-phase with the applied field. At high frequency, dipoles move very little before the applied electric field changes orientation, and thus there is insignificant contribution to ε', whereas at low frequency, the dipoles are fully displaced, and their net moment stays antiparallel with the field, resulting in the maximum ε'. Between the high and low frequencies exists a relaxation frequency, the reciprocal of a relaxation time constant, where the dipoles are maximally out of phase with the applied field, resulting in peak ε''. The Debye relaxation is the simplest form of relaxation where the rate of change of polarization is proportional to the instantaneous polarization and is usually associated with orientation relaxation. The Cole−Cole relaxation is formed by a log-normal distribution of Debye relaxations.

In this article, we use the term "permittivity" without modification to indicate the real part of the relative permittivity,

---

* To whom correspondence should be addressed. Tel: 720-240-0149. E-mail: dstillman@boulder.swri.edu.
† Southwest Research Institute.
‡ Colorado School of Mines.

TABLE 1: Soil Properties of the Measured Samples[a]

name	Sand	CPG	JSCM1	SAz
median grain size (μm)	110	37−74	200−500	<1
surface area (m^2/g)	0.1 ± 0.03	82.1	85.1 ± 4	73.9 ± 4
composition	quartz	SiO$_2$	major plagioclase feldspar, minor magnetite, <1% clay	Ca-montmorillonite

[a] Surface areas were obtained using nitrogen gas with the Brunauer, Emmett, and Teller (BET) method. The surface area of JSCM1 is so high because it is a palagonitic soil.

otherwise known as the dielectric constant. The loss tangent is defined as tan $\delta = \varepsilon''/\varepsilon'$, and the phase is $\tan^{-1}(\varepsilon'/\varepsilon'')$.

2.1. DC Conductivity of Ice and Hydrates. The electrical properties of ice−hydrate binary systems formed from frozen saline solutions were investigated by Grimm et al.[7] For salt concentrations in the initial liquid less than the eutectic composition, ice forms progressively during freezing, and the residual liquid becomes more saline until the eutectic temperature (222 K for CaCl$_2$) is reached, at which point the remaining liquid freezes to the eutectic composition of ice and salt hydrate. Above the eutectic temperature, the liquid fraction was found to form interconnected networks, brine channels, but only if the initial salt concentration was >3 mM. Brine channels were easily detectable because they increase DC conductivity by orders of magnitude and have relatively low apparent activation energies. Below the eutectic temperature, DC conductivity was found to be controlled by the conductivity of the salt hydrate, which was much lower than that of brine channels but much greater than that of ice.

2.2. Orientational Polarizability of Ice. Rotation and translation of protonic point defects (L and D Bjerrum defects, and H$_3$O$^+$ and OH$^-$ ionic defects) in the hydrogen-bonded ice lattice dominate the electrical properties of ice.[8] The net movement of either kind of defect has the effect of reorienting the permanent dipole of the H$_2$O molecule. The motions of these defects result in linked σ_{DC} and polarizability.[9,10] Bjerrum defects typically outnumber ionic defects, and thus Bjerrum defects control the dielectric properties, whereas the ionic defects control σ_{DC}. The frequency of the Debye dielectric relaxation of ice is a function of temperature and the number of Bjerrum defects. Ice always has some intrinsic defects, whereas extrinsic Bjerrum defects are created by lattice substitutions, typically Cl$^-$. The Cl$^-$ saturation limit of ∼0.3 mM (2.7 ppm)[11] creates an upper bound to the relaxation frequency.[7]

2.3. Adsorbed Water. Thin films of H$_2$O, typically measured in monolayers, are adsorbed by hydrogen bonds to the surfaces of solids.[1] Experimental data and molecular dynamics simulations have shown that hydronium ions are formed during adsorption.[12−15] Adsorption bonds weaken with the distance of water molecules from the solid surface. H$_2$O is adsorbed within two to three monolayers of the solid surface and remains adsorbed down to temperatures of at least 77 K.[16] Two dielectric relaxations have been previously directly identified with adsorbed water. The faster relaxation occurs between the relaxation frequencies of liquid water and ice.[7,17−21] This relaxation is due to the orientational polarization of the water molecule. Its relaxation frequency is between that of water and ice because the individual H$_2$O molecules are bonded stronger than in unbound liquid but weaker than in solid form. The second, slower, relaxation of adsorbed water occurs at a frequency below that of the rotational polarization of ice.[21−25] The strength of this relaxation increases markedly from one to two monolayers and then becomes nearly constant.[22,23] Sjöström et al.[21] suggested a Maxwell−Wagner interfacial polarization caused by a conductivity contrast between silicate and adsorbed water. The temperature dependence of the relaxation reverses (i.e., lower

relaxation frequency at higher temperature) above room temperature. Sjöström et al.[21] suggested this was caused by evaporation of the adsorbed water, whereas others[25−29] have called for a kinetic transition due to water molecule reorientation in the vicinity of a defect.

2.4. Anomalous Low-Frequency Dispersion. An anomalous low-frequency dispersion (LFD) has been measured for many minerals in the presence of humidity[30−33] and in high vacuum and high temperatures.[34] The LFD is generally evident as a gradual decrease in both ε' and ε'' over several decades or more in frequency and can create enhanced ε'' at frequencies <10 GHz. The dispersion can be modeled as a broad Cole−Cole dielectric relaxation[35] but has also been treated as approximately constant loss tangent.[30] The broadband nature of the LFD is generally thought to be caused by a wide distribution of activation energies for charge hopping.[32,33,36−38] The LFD is not likely a Maxwell−Wagner effect because the broad distribution of relaxation times would correspond to an unrealistically broad distribution of shape factors.[32,33]

3. Materials

Our silicate samples consisted of a very fine-grained sand (hereafter, "Sand"), a nanograin controlled-pore glass (CPG), a calcium-rich montmorillonite (SAz), and a palagonitic tephra (JSCM1). The sand (U.S. Silica OK-110) served as the baseline material. It has large pores and small specific surface area (A_s) compared with the other materials (Table 1). The CPG (Millipore CPG00240C) is a nonreactive and monomineralic silica, but it has A_s comparable to that of the montmorillonite and palagonitic tephra. SAz (Clays Repository SAz-1) was chosen to observe the electrical effect of surface reactivity in a monomineralic sample. JSCM1 was acquired from Johnson Space Center (JSC-Mars-1); it is the submillimeter fraction of tephra mined from Pu'u Nene, Hawaii. This sample was chosen as a polymineralic endmember with distributed pore sizes. It has been offered for laboratory study as a spectral analog to the martian surface,[39] although we have determined that its specific surface area is much higher (85.1 m^2/g) than that measured in situ on Mars (17 m^2/g).[40] Properties of our four silicate samples are summarized in Table 1.

4. Methods

4.1. Sample Preparation. To remove residual water, each silicate sample was first baked at 413 K (140 °C) and then vacuum-dried until its mass did not change over a 24 h period. The 3 cm wide by ∼0.3 cm thick cylindrical sample holder was loaded, and CaCl$_2$ solutions were added and mechanically mixed. The electrical properties of each silicate sample were first measured at 100% saturation to determine porosity. Because similar packing procedures were used for all samples of a particular material, the porosity was assumed to be constant; therefore, the relative volume fractions of silicate, saline solution, and air were readily determined.

CaCl$_2$ solutions were used to control brine, ice, and hydrate conductivity in the experiments. CaCl$_2$ was previously studied

Electrical Properties of Ice−Silicate Mixtures

J. Phys. Chem. B, Vol. 114, No. 18, 2010 **6067**

by Grimm et al.,[7] is geologically relevant, and has a low eutectic temperature (222 K), allowing clear discrimination of subeutectic and supereutectic behaviors. The use of deionized water alone can result in large variations in conductivity due to small amounts of extant salts in the silicates, so solutions of larger, known salinity were preferred for control. Initial salt concentrations of 1 and 100 mM were used to bracket the 3 mM concentration threshold, at which brine pockets form connected brine channels.[7]

Next, the sample holder was placed into a heavily insulated ultralow freezer (So-Low C85-9), maintained to within ±0.2 K using a Lakeshore 331 temperature controller. The temperature inside the freezer was held at 2° below the freezing point of the salt solution (271 K for 1 mM and 270 K for 100 mM CaCl$_2$) for 1 h to start crystallization and then at 10° below the freezing point for an additional 3 h. The temperature was then increased to 2° below freezing and maintained for 3 h to facilitate annealing. This process was then repeated at the eutectic temperature of 223 K (−50 °C). The temperature was then lowered to the minimum temperature of the freezer (~180 K) at a slow rate of 0.2 K/min to impede bubble and crack formation. The electrical properties of the sample were measured while the sample was warmed to negate any effects of supercooled water due to the lack of nucleation sites.[41] Measurements were taken at approximate logarithmic temperature intervals, except in the vicinity of the eutectic where smaller temperature increments were used.

4.2. Electrical Properties Measurements. Measurements were performed from 1 mHz to 1 MHz with a Solartron 1260A frequency response analyzer, 1296A dielectric interface (input impedance 10^{14} Ω), and a three-electrode (capacitively coupled) sample holder. The third grounded electrode is used to control electric-field geometry. The 1260A/1296A system is rated at better than 2% accuracy for a capacitance >1 pF; all of our measurements met this criterion. We converted complex impedances to electrical properties (complex permittivity or complex conductivity) using the electrode geometry.

For each spectrum, we used a nonlinear curve-fitting procedure to fit ε' and ε'' simultaneously to determine the parameters of up to four Cole−Cole dielectric relaxations, plus σ_{DC}

$$\varepsilon^* = \varepsilon_{HF} + \sum_i \frac{\Delta\varepsilon_i}{1 + (i\omega\tau_i)^{1-\alpha_i}} - \frac{j\sigma_{DC}}{\varepsilon_0\omega} \qquad (1)$$

where $\Delta\varepsilon_i$, τ_i, and α_i are the real permittivity contrast, relaxation time, and distribution parameter, respectively, for the ith dielectric relaxation, and ε_{HF} is the "high-frequency" real permittivity. A pure Debye relaxation would have $\alpha = 0$. Once τ and σ_{DC} were determined for each temperature, T, the temperature dependences were modeled using generalized Boltzmann distributions

$$\tau = \tau_o \, e^{E_\tau/kT} \qquad (2)$$

and

$$\sigma_{DC} = \sigma_o \, e^{-E_\sigma/kT} \qquad (3)$$
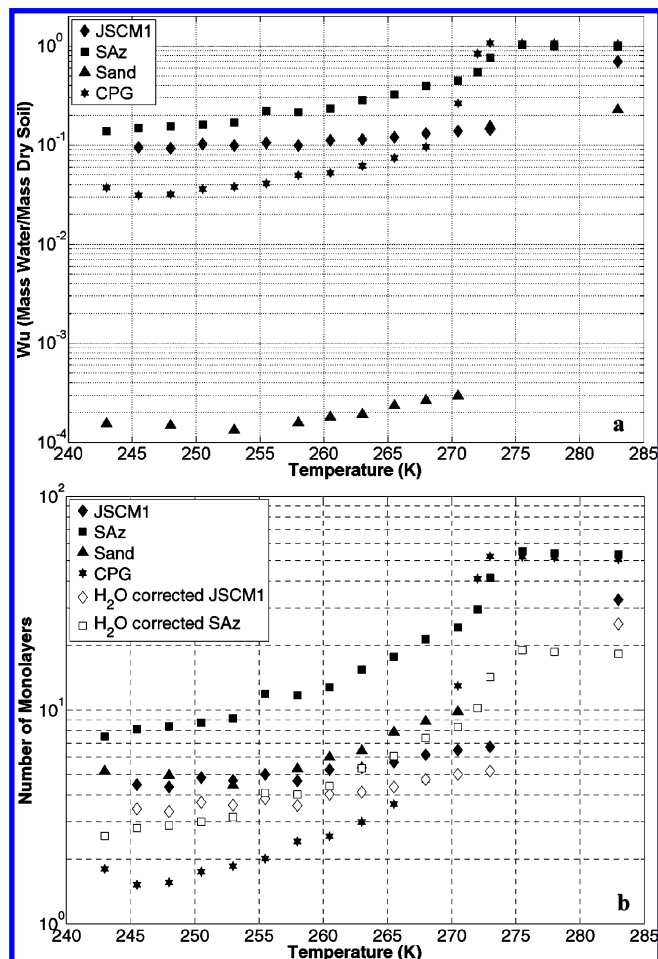
where k is Boltzmann's constant.

Figure 1. (a) Mass ratio of unfrozen water to dry silicates from NMR measurements using a 5.5 mol % D$_2$O solution in H$_2$O. (b) Number of equivalent monolayers based on surface areas in Table 1 (closed symbols). Number of equivalent monolayers based on H$_2$O-corrected surface areas (open symbols).[46]

4.3. Nuclear Magnetic Resonance Sample Preparation. NMR was used to measure the amount of unfrozen adsorbed water at subfreezing temperatures. The silicates were prepared by drying in an oven at 383 K for at least 1 week. Water added to the silicates was enriched in deuterium, ^{2}H or D, by the addition of D$_2$O to distilled H$_2$O to enhance the NMR response. Because of the rapid chemical exchange between D and H, the bulk of the D present in the enriched water is DHO. About 5.5 mol % D$_2$O was used. We prepared samples with excess water by weighing the dried silicates before and after the addition of water and mechanically mixing the water and solid. To minimize water evaporation during transfer of the water and solid mixture, the mixture was cooled to 253 K before transfer to the sample tube. Samples were transferred to the NMR sample container and weighed at 253 K prior to the NMR measurements.

4.4. Nuclear Magnetic Resonance Spectroscopy. All ^{2}H NMR spectra were recorded on a Chemagnetics Infinity 400 NMR spectrometer operating at 61.34 MHz for ^{2}H. A 5 mm nonspinning Chemagnetic ^{2}H probe is specifically designed for ^{2}H wide-line NMR experiments with its 5 mm detection solenoid perpendicular to the field. The radio frequency (rf) power output of the rf amplifier was adjusted to provide a 90° excitation pulse of 2.0 μs. All experiments used a solid echo (90°$_x$ − τ − 90°$_y$ − τ − acquisition) pulse sequence and a 2 MHz sweep width.[42] Spectra were recorded as a function of the half-echo time τ and extrapolated to τ = 0 to correct the signal intensity
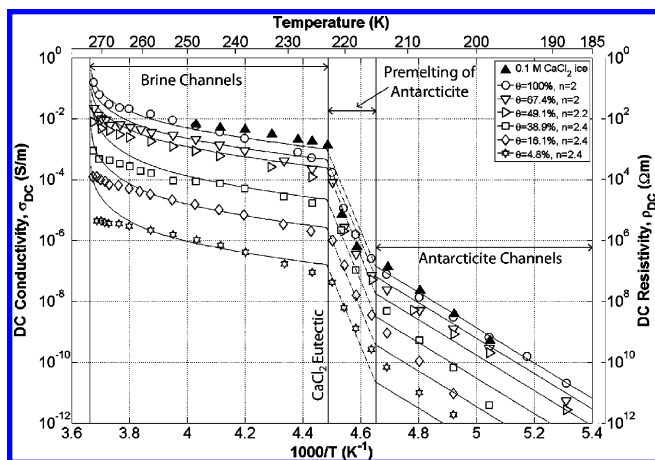
Figure 2. DC conductivity of fine-grained sand as a function of saturation with 0.1 M $CaCl_2$ solution with Archie's law fits shown by solid lines.

for the effect of spin–spin relaxation, T_2. Spin–lattice relaxation (T_1) values were measured by a progressive saturation[42] version of the solid echo pulse sequence. The number of signal acquisitions varied depending on the signal strength. Pulse delays between signal acquisitions also varied depending on T_1. The ^{2}H NMR resonance line due to unfrozen HDO in the samples was identified through both its T_1 and T_2 relaxation behaviors, appearing as a relatively sharp feature at the center of the spectrum.[43] The integrated intensity of this sharp ^{2}H resonance line (extrapolated to $\tau = 0$) is proportional to the amount of unfrozen HDO, and its relative amount was determined from an ^{2}H NMR measurement at 283 K of the sample, where all HDO is unfrozen and detected.

This spectrometer is equipped with a Chemagnetics solid-state temperature controller. The temperature was calibrated at the position of the probe using the chemical shift separation of the −OD and −CD$_3$ resonance lines of methanol-D$_4$, previously cross-calibrated to the temperature dependence of the proton chemical shift separation of −OH and −CH$_3$ of methanol.[44]

5. Results and Discussion

5.1. Unfrozen Water Content. We performed NMR measurements on all of the samples down to temperatures of 243

K to determine unfrozen water content (Figure 1a). The mean number of H_2O monolayers, n_m, is defined by

$$n_m = \frac{W_u}{A_s \rho_w h_m} \quad (4)$$

where W_u is the mass ratio of unfrozen water to the mass of dry soil, A_s is the specific surface area (m^2/g), ρ_w is the density of unfrozen water (g/m^3), and h_m is the thickness of an H_2O monolayer, ~0.25 nm.[45] The asymptotic behavior in Figure 1b suggests that two to eight monolayers of adsorbed water exist at low temperatures. Surface areas were measured by the classical BET method using nitrogen gas. However, water can penetrate the interlayer spaces of clays, increasing the active surface area of montmorillonite by 190% and JSCM1 by 30%.[46] With these corrected surface areas, the NMR results are consistent with just two to three monolayers of adsorbed water on average.

5.2. DC Conductivity. Various amounts of the $CaCl_2$ solutions were mixed with sand to determine how σ_{DC} varies with concentration and saturation (Figure 2). The initial liquid saturation θ is expressed relative to the pore volume. The DC conductivity for 0.1 M $CaCl_2$ solutions can be divided into several different regions by temperature. At low temperatures (<216 K), σ_{DC} has an intermediate activation energy, $E_a^{DC} \approx$ 1.2 eV, and is dominated by channels of antarcticite ($CaCl_2 \cdot 6H_2O$), just as was measured in ice samples.[7] As the sample was heated to near the eutectic temperature, these antarcticite channels began to premelt or form quasi-liquid films below the melting point. This sharply increased σ_{DC} in a region of high apparent $E_a^{DC} \approx 4$ eV. Above the eutectic, brine channels form that have a low apparent $E_a^{DC} \approx 0.4$ eV; near the freezing point, σ_{DC} again increases rapidly.

Grimm et al.[7] showed that the brine-channel conductivity in saline ices can be modeled as a variation in conductivity with liquid volume following Archie's law.[47] Here we expand this approach to the entire measured temperature range and ice–silicate mixture
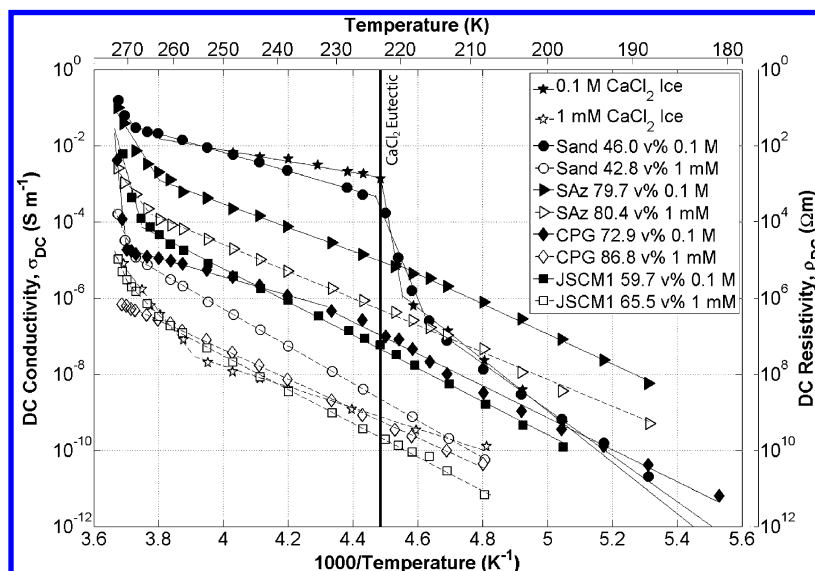

Figure 3. DC conductivity of ice and mixtures of sand, CPG, SAz, and JSCM1 with 0.1 M and 1 mM solutions of $CaCl_2$.
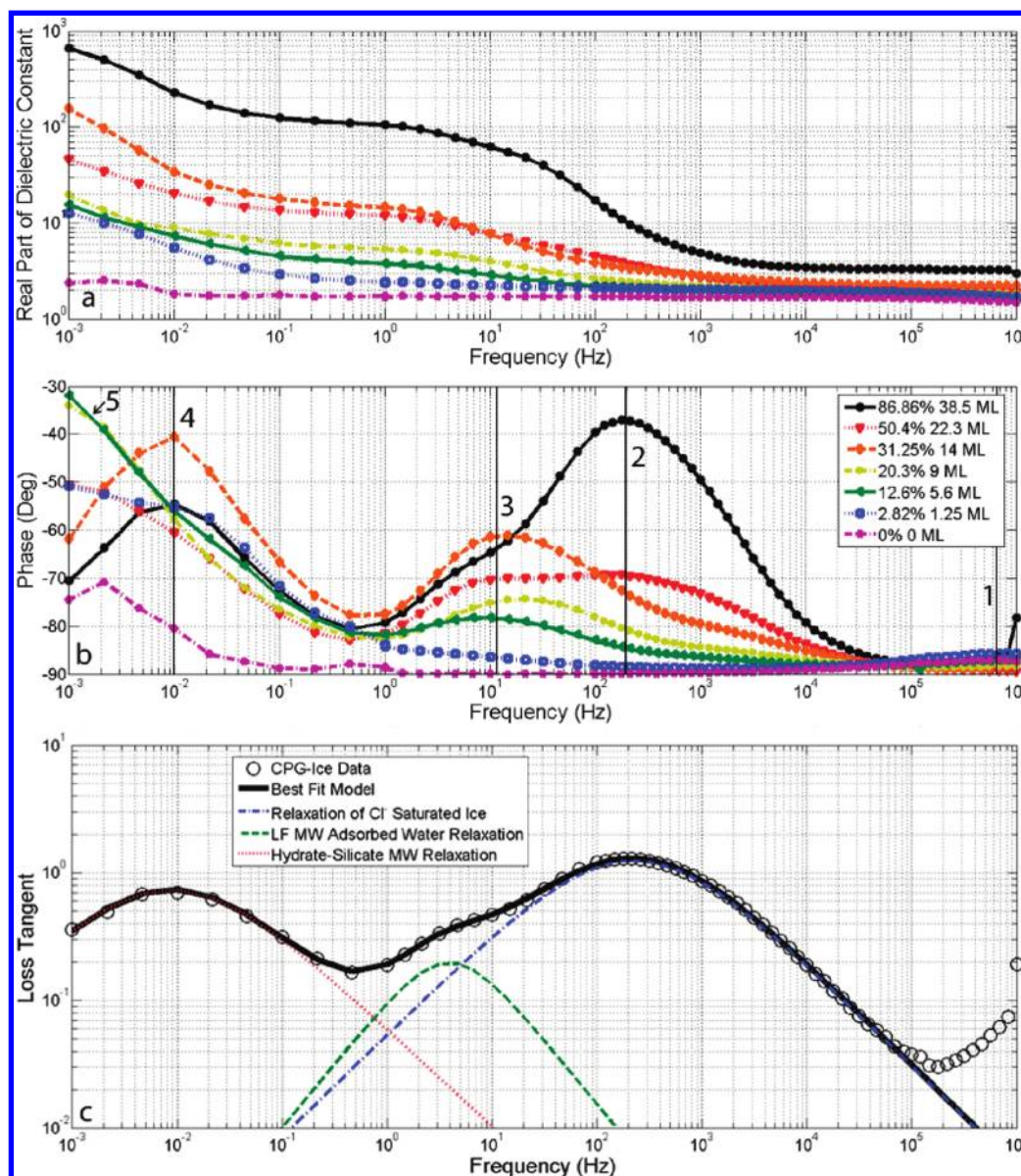
Figure 4. Five relaxations (1, adsorbed water; 2, ice relaxation; 3, low-frequency Maxwell−Wagner adsorbed water relaxation; 4, hydrate-silicate Maxwell−Wagner relaxation; 5, LFD) of CPG as a function of 1 mM $CaCl_2$ saturation at ~181 K. The strength of the ice relaxation decreases markedly with decreasing water fraction, but the low-frequency Maxwell−Wagner adsorbed water and hydrate-silicate Maxwell−Wagner relaxations only change slowly, confirming their tie to silicate surface area and not pore volume. The LFD is illustrated by the increase in real permittivity and phase in ≤20.3 vol % H_2O. (a) Real permittivity. (b) Phase angle. (c) Modeling of three relaxations at 181.4 K for 86.86 vol % H_2O.

$$\sigma_{DC} = \sigma_{DC}^{cond} \phi^m S_{cond}^n \qquad (5)$$

where σ_{DC}^{cond} is the DC conductivity of the conductive phase, S_{cond} is the relative saturation (fractional saturation of the pore volume by the conductive phase), and m is the cementation exponent of the conductive phase. Brine is considered to be the conductive phase for $T > 223$ K and hydrate for $T < 215$ K. No fitting was done of the intermediate antarcticite premelting regime. The temperature-dependent relative saturations and conductivities σ_{DC}^{brine} and $\sigma_{DC}^{hydrate}$ were determined from the binary phase diagram. (See the Appendix.) Note that $S_{cond} < \theta$ because frozen liquid above the eutectic temperature and ice below the eutectic temperature are considered nonconductive. From the saturated sample, the porosity, ϕ, was determined to be 46%, and the cementation exponent, m, was ~2, which is in good agreement with the expected value for sand.[48]

The only remaining unknown is the saturation exponent, n. Remarkably, each curve of constant initial θ consistently fits

above and below the eutectic temperature using the same n (Figure 2). At large θ, n is close to the typical value of 2 (ref 49), but n increases as θ falls, approaching 2.4 for $\theta < 40\%$. We interpret this increase in the rate of change of conductivity with decreasing initial saturation to represent an increase in tortuosity in the brine and hydrate channels.

In contrast, the 1 mM $CaCl_2$ solution in sand showed no evidence of brine channels or an abrupt change to salt hydrate conduction below the eutectic (Figure 3). This is consistent with the finding by Grimm et al.[7] that brine channels in saline ice become discontinuous below concentrations of 3 mM. Therefore, σ_{DC} of 1 mM $CaCl_2$ solutions is dominated by the conductivity of ice.

In samples SAz, CPG, and JSCM1, σ_{DC} does not show the characteristic brine-channel jump at 100 mM, which is well above the 3 mM threshold (Figure 3). This can also be interpreted in light of previous saline−ice measurements. Grimm et al.[7] calculated that the 3 mM threshold corresponded to a

6070 *J. Phys. Chem. B, Vol. 114, No. 18, 2010*
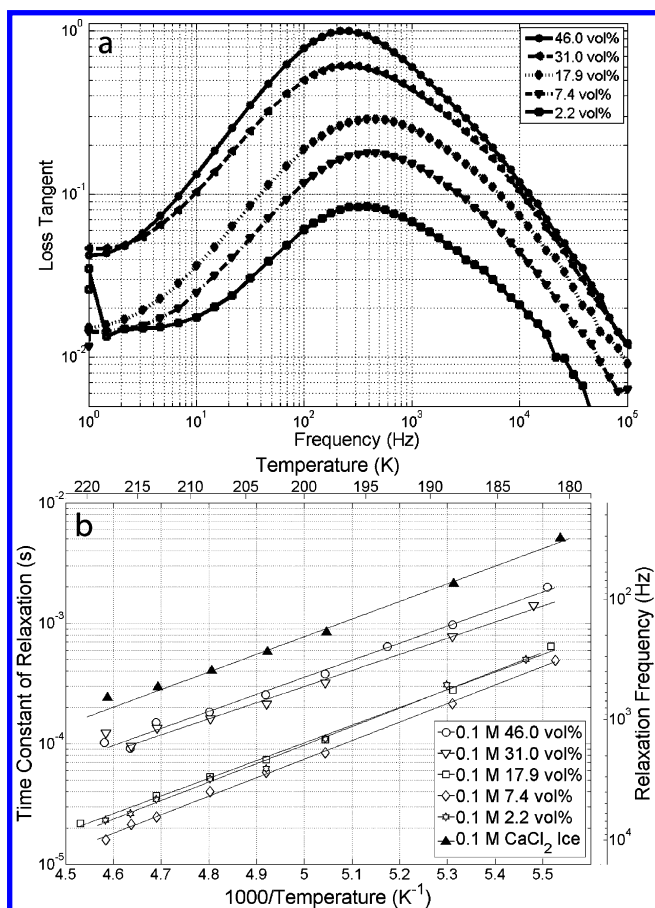
Stillman et al.

Figure 5. Ice relaxation in sand. The shorter relaxation times compared to silicate-free ice are likely due to Cl⁻ supersaturation in proximity to pore walls. (a) Loss tangent versus frequency for various values of ice vol % with 0.1 M CaCl₂. (b) Time constant of relaxation versus temperature for the dielectric relaxation of ice.

Figure 6. Dielectric mixing in sand-ice mixtures with 0.1 M CaCl₂. (a) Permittivity, dominated by ice relaxation. (b) Power law mixing model for static permittivity. Best fit exponent 2.7 ± 0.3 implies ice content can be determined to ~2% in these mixtures.

brine-channel width of a few micrometers. Large capillary pressures in these small pores segregate remaining fluid, disconnecting electrical pathways. The small pore sizes for CPG and SAz always lead to high capillary pressures, disconnecting brine channels regardless of their concentration. We infer that the small size fraction in JSCM1 fills the larger pore throats and similarly controls brine-pocket geometry.

The DC conductivities of CPG and JSCM1 are similar at the same initial salt concentration. This is further evidence that the principal conductivity pathway is through the ice. However, σ_{DC} of SAz is approximately three orders of magnitude higher than CPG and JSCM1, far too high for ice. The high σ_{DC} likely arises from surface charges, specifically interlayer cation mobilization due to adsorbed water.

5.3. Dielectric Relaxations. We identified five dielectric relaxations in subfreezing silicate-ice mixtures (Figures 4 and 8 and Figures S1−S4 in the Supporting Information). Two of these relaxations are interpreted as the reorientation of the electrical dipole of the H₂O molecule in ice and in adsorbed water, respectively. Two others are likely Maxwell−Wagner interfacial polarizations, whose origin we investigate using activation energies and dependence on initial H₂O content. The last relaxation is the LFD signature. The reorientation and Maxwell−Wagner interfacial polarization of adsorbed water are only observed in samples with large surface areas.

5.3.1. Orientational Polarization of Adsorbed Water. The fastest relaxation (630 kHz at 181 K) has an activation energy of 0.4 eV and is only detected in the high-surface area
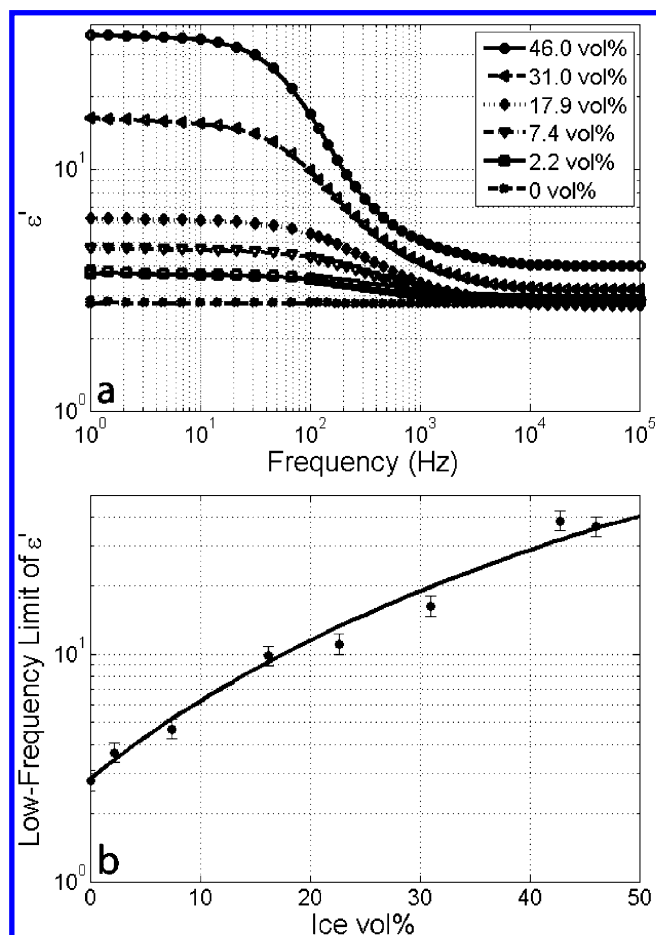
samples SAz (Figure S3 in the Supporting Information), CPG (Figure 4), and JSCM1. This relaxation lies well above the ice relaxation but is also many decades below the relaxation frequency for free-water rotation. This indicates that the bond strength between solid and liquid H₂O lies between those in homogeneous liquid or solid. From these observations, this relaxation can be identified as the orientational polarization of adsorbed water.[21,24−29,50]

5.3.2. Orientational Polarization of Ice. The second highest frequency relaxation (200 kHz at 181 K) is readily identified as the orientational polarization of adsorbed water because it has an activation energy 0.29 eV, and when fully saturating, the porosity has a similar relaxation frequency to that of bulk ice. The magnitude of the ice dielectric relaxation $\Delta\varepsilon$ varies directly with the amount of ice in the sample and varies weakly inversely with the absolute temperature (Figure 5a and Figures S1−S4 in the Supporting Information). The relaxation frequency depends on temperature as well as the number of ice-lattice defects (extrinsic L defects),[8] here created by Cl⁻ (Figure 5b).

We wished to determine how well ice content of a sample could be recovered from dielectric properties. Therefore, the low-frequency limit of ε' (Figure 6a) was modeled with a three-phase power law

$$\varepsilon_s^{1/\gamma} = \phi_{sand}\varepsilon_{sand}^{1/\gamma} + \phi_{ice}\varepsilon_{ice}^{1/\gamma} + \phi_{air}\varepsilon_{air}^{1/\gamma} \quad (6)$$

where ε_s is the static permittivity, ϕ is the volume fraction of a phase, and γ is the power-law exponent. Commonly, $\gamma = 1-3$,

Electrical Properties of Ice−Silicate Mixtures

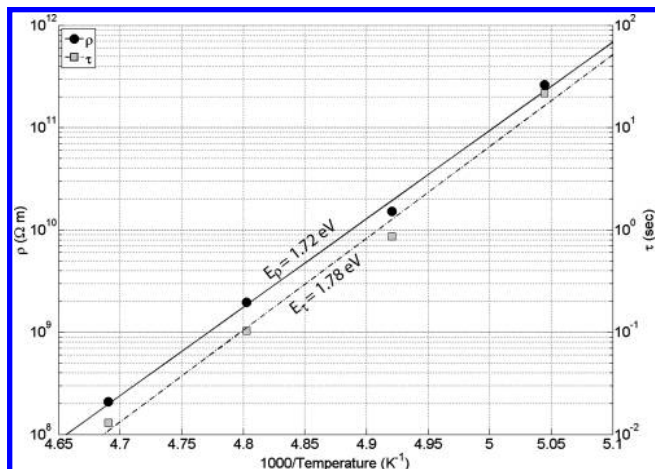*J. Phys. Chem. B, Vol. 114, No. 18, 2010* **6071**

Figure 7. Arrhenius plot of resistivity ρ and τ for 17.9 vol % ice mixed with sand. Resistivity is used here instead of DC conductivity so that both fits showed increasing slopes. The similar activation energies suggest that this relaxation is created by a Maxwell−Wagner interfacial polarization of conductive antarcticite ($CaCl_2$ hydrate) surrounded by resistive silicates.
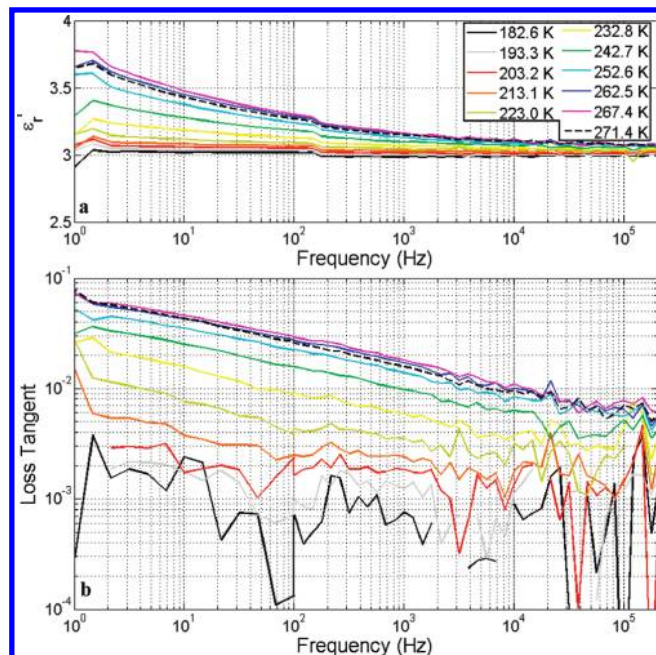

Figure 8. LFD in "dry" sand, interpreted here as a signature of water that adsorbed on a sample that was previously dried in thermal vacuum. (a) Real permittivity versus frequency. (b) Loss tangent versus frequency. This slope of the loss tangent is too shallow to be caused by DC conductivity, which would plot with a slope of −1. The noise level in loss tangent is ∼0.003.

with the Maxwell Garnet model approximated at $\gamma = 1$, the complex refractive index model equivalent to $\gamma = 2$, and the Looyenga model with $\gamma = 3$ (ref 51). For sand−ice mixtures, the best fit was $\gamma = 2.7 \pm 0.3$ (Figure 6b), and the scatter indicates that the ice content can be inverted from static permittivity to ±5%. This result contrasts with two previous attempts to invert ice content from ice−silicate mixtures. Alvarez[52] found two regions of linear dependence between the logarithm of the maximum ε'' and ice content by weight at 100 K. However, he only measured down to 30 Hz, and at 100 K, the relaxation frequency of ice is ≪1 Hz. Therefore, this response was not ice but possibly the orientational relaxation of adsorbed water. Bittelli et al.[53] addressed the frequency−temperature range for terrestrial permafrost (100 Hz to 200 kHz for 243−278 K), but the high conductivity of these clay-rich loess soils prevented measurement of static permittivity.

The ice relaxation frequency in the sand mixtures increases with decreasing ice concentration (Figure 5), requiring an increasing relative density of lattice defects where ice fills a smaller proportion of the pore volume. Furthermore, the relaxation frequencies always exceed those of chloride-saturated, silicate-free ice,[7] indicating that the defect density in ice mixed with silica is always greater than that in ice alone. Finally, because the orientational polarization of ice is a Debye relaxation ($\alpha = 0$), the broader Cole−Cole relaxation $\alpha = 0.24$ points to a process with a longer length scale than isolated defect rotation. These behaviors indicate that silica surfaces influence defect density in ice. We suggest that the additional defects are either caused directly by electric fields near the silica surfaces or indirectly by supersaturation of Cl^- in the ice lattice. For the latter interpretation, Jaccard theory[10] indicates that the supersaturated ice would contain ∼21 ppm chloride compared with just 2.7 ppm for Cl^- saturation.

5.3.3. Hydrate-Silicate Maxwell−Wagner Interfacial Polarization. This relaxation (Figure 4 and Figures S2 and S4 in the Supporting Information) has an activation energy that is nearly the same as that observed for σ_{DC} (Figure 7). Because salt hydrates are the dominant DC conductor in frozen saline ices,[7] but without any interfacial polarizations, the relaxation observed here must be associated with charge motion in the salt hydrates that is terminated by silicate boundaries. Therefore, the relaxation frequency and σ_{DC} both decrease with decreasing

temperature because free charges are less mobile and take longer to build up on an interface.

5.3.4. Adsorbed Water Maxwell−Wagner Interfacial Polarization. This relaxation was only detected in the high surface area samples SAz (Figures S1−S3 in the Supporting Information), CPG (Figure 4), and JSCM1. Its activation energy is 0.4 eV (equal to that of the orientational adsorbed water relaxation), and it was slower than the ice relaxation at 183 K. Therefore, this relaxation can be identified as another signature of adsorbed water.[7,16−21] Sjöström et al.[21] suggested a Maxwell−Wagner interfacial polarization due to a conductivity contrast between the silicate and the adsorbed water, with a reverse in temperature dependence caused by evaporation. We support this conclusion by observing that the relaxation shifts to lower frequencies with time when the sample is at constant temperature under ambient (low-humidity) conditions (Figure S5 in the Supporting Information). We interpret the mechanism of this polarization below, jointly with the LFD.

5.3.5. Anomalous Low-Frequency Dispersion (LFD). A broad, temperature-dependent dielectric relaxation or dispersion occurs in all measured samples with <2 vol % H_2O (Figures 8 and Figure S3 in the Supporting Information). This signature is weak and therefore was probably obscured at larger H_2O concentrations. It also has the same general shape among the different samples ($\alpha \approx 0.75 \pm 0.07$). These trends in permittivity require a very high ε_s, but it is not well-characterized because the relaxation frequency is always below our lower measurement of limit of 1 mHz. This also makes it difficult to estimate the activation energy.

Two further observations in our experiments argue for an effect of adsorbed water. First, the LFD is observed in monomineralic sands with negligible conductivity. Therefore, the effect cannot arise from within the silicate. Second, the LFD is continuous across both freezing and eutectic temperatures, so it is not unique to either bulk liquid or frozen saline H_2O
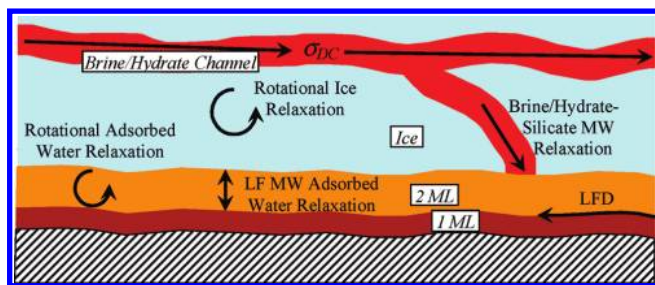
Figure 9. Sketch of the five dielectric relaxations and DC conductivity (σ_{DC}) measured in ice−silicate mixtures. DC conductivity occurs when brine channels exist throughout the entire sample. If these brine channels are cutoff, then free charges build at the interface creating a Maxwell−Wagner (MW) relaxation. The intrinsic dipole of water creates rotational relaxations in ice and >1 monolayer of adsorbed water. The translational movement of H_3O^+ ions in the adsorbed water layer creates a low-frequency MW relaxation. The longitudinal hopping of H_3O^+ ions in the adsorbed water layer creates the LFD.

but again must be associated with a ubiquitous phase, the unfrozen layer.

5.4. Charge-Transport Mechanisms in Adsorbed Water. Our experiments have shown that subeutectic low-frequency ice-silicate electrical properties can be summarized as DC conductivity dominated by hydrates, one relaxation in ice, one hydrate-silicate interaction, and three adsorbed-water signatures: an orientational polarization, an interfacial polarization, and the LFD. Charge transport in ice[10] and hydrates[9] has been understood in terms of protonic point defects. Rotation of H_2O causes the adsorbed-water orientational polarization.[21] We suggest that protons (hydronium ions) are the most likely charge carriers responsible for the adsorbed-water interfacial polarization and LFD. Two arguments support this claim. First, these relaxations occur even when the adsorbed water is deionized (Figure S3 in the Supporting Information). Second, the affinity of hydronium for the adjacent surface makes interfacial water slightly acidic,[12−15] providing mobile protons. Proton motion thus provides a unifying foundation for the electrical behavior of adsorbed water through rotation (around oxygens) and both transverse and longitudinal translation with respect to the layer (Figure 9). The last is likely a hopping mechanism[30,33] because the very broad frequency range for the dispersion is not compatible with any reasonable Maxwell−Wagner mechanism.[32]

6. Conclusions

Our measurements of ice−silicate mixtures have revealed new electrical signatures, while also reproducing previous results from the literature. Our selection and control of sample materials allowed us to assign unique mechanisms to each of these signatures. DC conductivities indicate that brine channels can persist even at small volume concentrations (∼1%) in soil pore spaces. However, when the pore sizes in the soil become too small (about micrometers), the brine channels become isolated and disconnected. Although brine channels could not form in a fine-grained montmorillonite, SAz, enhanced DC conductivity was found compared with other materials of similar specific surface area. We attribute this to proton mobility in thin films of H_2O in the swelling clay interlayers.

The DC conductivities of sand−ice mixtures were well fit by the classical Archie law with partial saturation of the conducting phase. Above the eutectic temperature, brine channels are the principal conductors, whereas salt hydrate (here, antarcticite) is the main conductor at subeutectic temperatures. The parameter describing pore geometry is consistent with

values expected for sands. At fixed H_2O saturation, the parameter that describes saturation geometry is remarkably constant with temperature, specifically across the eutectic, which confirms that brine channels become hydrate connections. As saturation decreases, increasing tortuosity in the conductive phases is indicated.

Five dielectric relaxations were identified and measured in the ice−silicate mixtures, which are summarized in order of decreasing relaxation frequency at 181 K.

The first relaxation is due to the rotation of adsorbed water. This orientational relaxation occurs at the highest frequency in our temperature range (∼630 kHz at 181 K) as the water molecule is bonded less tightly than ice.

The second relaxation is due to the rotation of protonic L-Bjerrum defects in ice (∼200 Hz at 181 K). The dielectric strength of the ice relaxation does not appear to be altered when ice is mixed with silicates. However, the relaxation frequency shifts to slightly higher frequencies, and the relaxation distribution broadens with decreasing ice content. This indicates that the ice nearest the pore walls has an excess of defects compared with that expected for chloride saturation. We suggest that Cl^- supersaturation may be caused by stronger electric fields near the silica surface, which reduce the amount of impurities that can be excluded during ice freezing.

The third relaxation is due to a Maxwell−Wagner interfacial polarization within adsorbed water (∼10 Hz at 181 K). When an external electric field is present, the hydronium ions that are preferentially found in the first monolayer of adsorbed water[12−15] can move across the second and third monolayers. The hydronium ions then build up and create a "transverse" interfacial polarization.

The fourth relaxation (10 mHz at 181 K) is caused by the Maxwell−Wagner interfacial polarization between salt hydrate and silicate, identified by having the same activation energy as σ_{DC}. This relaxation does not occur in saline ice because the hydrate is always interconnected.

The fifth relaxation is the LFD. This signature was observed in all samples at low water content. It is believed to be present but obscured at high water content. The LFD has been ascribed to a very broad distribution of hopping and tunneling rates, too broad for a Maxwell−Wagner interfacial polarization. The ubiquity of the LFD in our own experiments regardless of silicate grain size or composition, plus the evidence that all relevant measurements in the literature were performed under atmospheric conditions, strongly suggests that the LFD arises from the adsorbed-water layer. We further suggest that hydronium is the active charge carrier and migrates by hopping "longitudinally" along the liquid-like layer.

Supporting Information Available: Electrical properties as a function of temperature and frequency. This material is available free of charge via the Internet at http://pubs.acs.org.

Appendix

The σ_{DC}^{brine} was determined by calculating σ_{DC} of the brine at 293 K, $\sigma_{DC}^{brine@293}$, and then using an Arrhenius relationship with an activation energy of 0.114 eV (CRC, 2008) to correct

Electrical Properties of Ice−Silicate Mixtures

J. Phys. Chem. B, Vol. 114, No. 18, 2010 **6073**

$\sigma_{DC}^{brine@293}$ to the desired temperature (eq A1). The $\sigma_{DC}^{brine@293}$ (eqs A2 and A3) is a function of temperature because as the 0.1 M $CaCl_2$ decreases below its freezing point, it becomes concentrated in $CaCl_2$.

$$\sigma_{DC}^{brine} = \sigma_{DC}^{brine@293} \exp\left((-0.114/k)\left(\frac{1}{T} - \frac{1}{293}\right)\right) \quad (A1)$$

$$\sigma_{DC}^{brine@293} =$$
$$10^{-46.09 \log(p)^2 + 69.64(\log(p)) + 16.24/\log(p)^2 - 48.81(\log(p)) + 84.91} \quad (A2)$$

$$p = -2.165 \times 10^{-8}T^6 + 3.179 \times 10^{-5}T^5 -$$
$$1.9438 \times 10^{-2}T^4 + 6.335 \times 10^{-3}T^3 - 1160.5 \times 10^3 T^2 +$$
$$1.1332 \times 10^5 T - 460726.38 \quad (A3)$$

The $\sigma_{DC}^{hydrate}$ was determined from the results of Grimm et al.[7] (eq A4).

$$\sigma_{DC}^{hydrate} = 5.0 \times 10^{23} \, e^{-1.15/kT} \quad (A4)$$

References and Notes

(1) Sposito, G.; Prost, R. *Chem. Rev.* **1982**, *82*, 554.
(2) Benatov, L.; Wettlaufer, J. S. *Phys. Rev. E* **2004**, *70*, 061606.
(3) Dash, J. G.; Rempel, A. W.; Wettlaufer, J. S. *Rev. Modern Phys.* **2006**, *78*, 695.
(4) Williams, P. J.; Smith, M. W. *The Frozen Earth: Fundamentals of Geocryology*; Cambridge University Press: Cambridge, U. K., 1989.
(5) Davis, N. *Permafrost: A Guide to Frozen Ground in Transition*; University of Alaska Press: Fairbanks, AK, 2001.
(6) Scott, W. J.; Sellman, P. V.; Hunters, J. A. In *Geotechnical and Environmental Geophysics*; Ward, S. H., Ed.; Society of Exploration Geophysicists: Tulsa, OK, 1990; Vol. 1, pp. 355−384.
(7) Grimm, R. E.; Stillman, D. E.; Dec, S. F.; Bullock, M. *J. Phys. Chem. B* **2008**, *112*, 15382.
(8) Petrenko, V. F.; Whitworth, R. W. *Physics of Ice*; Oxford University Press: New York, 1999.
(9) Jaccard, C. *Helv. Phys. Acta* **1959**, *32*, 89.
(10) Jaccard, C. *Phys. Kondens. Mater.* **1964**, *3*, 99.
(11) Moore, J. C.; Reid, A. P.; Kipfstuh, J. *J. Geophys. Res.* **1994**, *99*, 5171.
(12) Nogami, M.; Abe, Y. *Phys. Rev. B* **1997**, *55*, 12108.
(13) Nogami, M.; Nagao, R.; Wong, C. *J. Phys. Chem. B* **1998**, *102*, 5772.
(14) Mahadevan, T. S.; Garofalini, S. H. *J. Phys. Chem. C* **2008**, *112*, 1507.
(15) Mahadevan, T. S.; Garofalini, S. H. *J. Phys. Chem. B* **2007**, *111*, 8919.
(16) Pearson, R. T., W; Derbyshire, *J. Colloid Interface Sci.* **1973**, *46*, 232.
(17) Hasted, J. B. *Aqueous Dielectrics*; Chapman and Hall: London, 1973.
(18) Hoekstra, P.; Delaney, A. J. *J. Geophys. Res.* **1974**, *79*, 1699.
(19) Ishida, T.; Makino, T.; Wang, C. *Clays Clay Miner.* **2000**, *48*, 75.
(20) Arcone, S.; Grant, S.; Boitnott, G.; Bostick, B. *Geophys.* **2008**, *73*, J1.
(21) Sjöström, J.; Swenson, J.; Bergman, R.; Kittaka, S. *J. Chem. Phys.* **2008**, *128*, 154503.
(22) McCaffety, E.; Zettlemoyer, A. C. *Discuss. Faraday Soc.* **1971**, *52*, 239.
(23) Bergman, R.; Swenson, J. *Nature* **2000**, *403*, 283.
(24) Spanoudaki, A.; Albela, B.; Bonneviot, L.; Peyrard, M. *Eur. Phys. J. E* **2005**, *17−27*, 21.
(25) Kinka, M.; Banys, J.; Macutkevic, J.; Poppl, A.; Bohlmann, W.; Umamaheswari, M.; Hartmann, M.; Volkel, G. *Phys. Status Solidi B* **2005**, *242*, R100.
(26) Gutina, A.; Axelrod, E.; Puzenko, A.; Rysiakiewicz-Pasek, E.; Kozlovich, N.; Feldman, Y. *J. Non-Cryst. Solids* **1998**, *302*, 235.
(27) Ryabov, Y.; Gutina, A.; Arkipov, V.; Feldman, Y. *J. Phys. Chem. B* **2001**, *105*, 1845.
(28) Frunza, L.; Kosslick, H.; Frunza, S.; Schönhals, A. *J. Phys. Chem. B* **2002**, *106*, 9191.
(29) Frunza, L.; Kosslick, H.; Pitsch, I.; Frunza, S.; Schönhals, A. *J. Phys. Chem. B* **2005**, *109*, 9154.
(30) Jonscher, A. K. *Philos. Mag. B* **1978**, *38*, 587.
(31) Bergman, R.; Swenson, J.; Borjesson, L.; Jacobsson, P. *J. Chem. Phys.* **2000**, *113*, 357.
(32) Shahidi, M.; Hasted, J. B.; Jonscher, A. K. *Nature* **1975**, 258.
(33) Jonscher, A. K. *J. Phys. D: Appl. Phys.* **1999**, *32*, R57.
(34) Carrier, W. D., III; Olhoeft, G. R.; Mendell, W. Physical Properties of The Lunar Surface. In *Lunar Sourcebook: A User's Guide to the Moon*; Heiken, G. H., Vaniman, D. T., French, B. M., Eds.; Cambridge University Press: New York, 1991; p 475.
(35) Stillman, D. E.; Olhoeft, G. R. *J. Geophys. Res.* **2008**, *113*, E09005.
(36) Dissado, L. A.; Hill, R. M. *J. Chem. Soc., Faraday Trans. II* **1984**, *80*, 291.
(37) Ngai, K. L.; Jonscher, A. K.; White, C. T. *Nature* **1979**, *277*, 185.
(38) Dyre, J. C.; Schroder, T. B. *Rev. Mod. Phys.* **2000**, *72*, 873.
(39) Allen, C. C.; Morris, R. V.; Lindstrom, D. J.; Lindstrom, M. M.; Lockwood, J. P. In *Lunar and Planetary Science Conference XXVIII*; Lunar and Planetary Institute: Houston, TX, 1997; p 1797.
(40) Ballou, E. V.; Wood, P. C.; Wydeven, T.; Lehwalt, M. E.; Mack, R. E. *Nature* **1978**, *217*, 644.
(41) *Clathrate Hydrates of Natural Gases*, 3rd ed.; Sloan, E. D., Koh, C. A., Eds.; CRC Press: Boca Raton, FL, 2008.
(42) Fukushima, E.; Roeder, S. B. W. *Experimental Pulse NMR: A Nuts and Bolts Approach*; Addison-Wesley Publishing Co., Inc.: London, 1981.
(43) Sparrman, T.; Oquist, M.; Klemedtsson, L.; Schleucher, J.; Nilsson, M. *Environ. Sci. Technol.* **2004**, *38*, 5420.
(44) Geet, A. L. v. *Anal. Chem.* **1970**, *42*, 679.
(45) Opitz, A.; Scherge, M.; Ahmed, S. I. U.; Schaefer, J. A. *J. Appl. Phys.* **2007**, *101*, 064310.
(46) Jänchen, J.; Bish, D. L.; Hellwig, U. In *40th Lunar and Planetary Science Conference*; Lunar and Planetary Institute: The Woodlands, TX, 2009.
(47) Han, M.; Youssef, S.; Rosenberg, E.; Fleury, M.; Levitz, P. *Phys. Rev. E* **2009**, *79*, 031127.
(48) Lesmes, D. P.; Friedman, S. Relationships between the Electrical and Hydrogeological Properties of Rocks and Soils. In *Hydrogeophysics*; Springer: New York, 2005.
(49) Sharma, P. V. *Geophysical Methods in Geology*, 2nd ed.; PTR Prentice Hall: Englewood Cliffs, NJ, 1986.
(50) Rotenberg, B.; Cadéne, A.; Dufrêche, J.-F.; Durand-Vidal, S.; Badot, J.-C.; Turq, P. *J. Phys. Chem. B* **2005**, *109*, 15548.
(51) Sihvola, A. *Electromagnetic Mixing Formulas and Applications*; Inst. Elec. Eng.: London, 1999.
(52) Alvarez, R. *Earth Planet. Sci. Lett.* **1973**, *20*, 409.
(53) Bittelli, M.; Flury, M.; Roth, K. *Water Resources Res.* **2004**, 40.